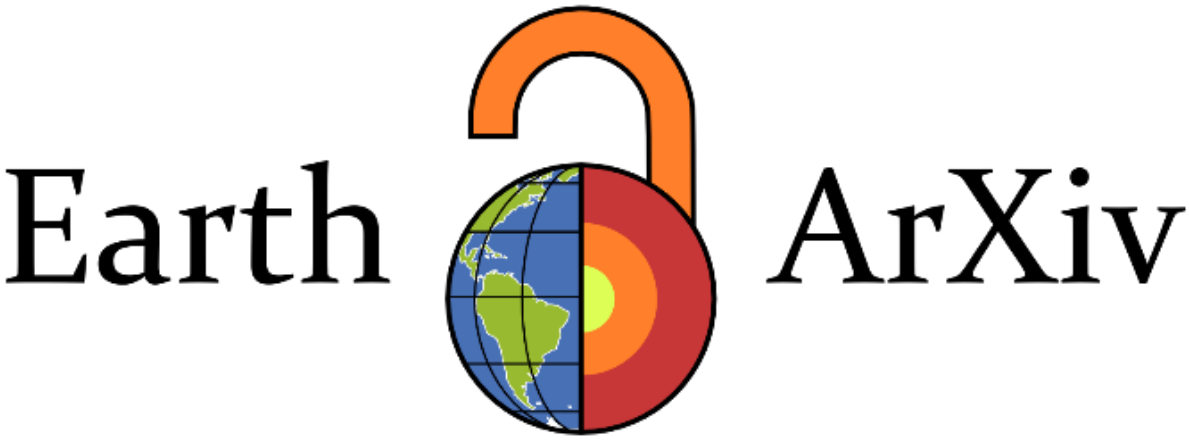

Experimental Investigation of Movement and Deposition of Woody-Debris Suspensions in Inclined Channel Tests

Chyan-Deng Jan and Le-Trang Nguyen *

Department of Hydraulic and Ocean Engineering, National Cheng Kung University, Taiwan

*Corresponding author: nltrang217@gmail.com

ABSTRACT

Debris flows, which mobilize large volumes of water, sediment, and woody debris, pose significant risks to human communities and infrastructure. In wildfire-affected forested areas, the accumulation of woody debris in drainage channels is exacerbated, thereby increasing the potential for more hazardous debris flows. To examine the influence of woody debris on debris flow dynamics, an inclined channel test, allowing the observation of woody debris flow in an inclined channel and its deposition in a horizontal tank, was conducted with highly concentrated woody-debris suspensions composed of clay, silt, woody debris, and water. This study explores how variations in fine-sediment fraction (C_{vf}), woody debris proportion (C_{vg}), and woody debris size (S_w) impact flow behavior, including the entry speed (V_0) into the horizontal tank, and deposition characteristics such as runout distance (L_R), deposit width (W_R), deposit thickness (H_R), and final profiles on a 20^o channel slope. To examine the influence of proportions and sizes of woody debris on the entry speed, an empirical equation is presented relating V_0 to C_{vf}, C_{vg}, and S_w using multiple linear regression analysis. The results indicate that a higher C_{vf} and C_{vg} yields smaller entry speeds, leading to shorter runout distances, thicker deposits, and wider deposit extents. The tests of larger S_w generate larger entry speeds, resulting in longer runout distances while producing thinner and narrower deposits. Empirical equations relating V_0 to L_R and W_R are also provided to further demonstrate the influence of entry speeds on the deposit characteristics. Additionally, a strong correlation was found between inclined channel test parameters (e.g., entry speed, runout distance, and maximum deposit width) and rheological parameters (e.g., yield stress and viscosity), suggesting that rheological properties can be indirectly estimated from inclined channel tests. These findings offer valuable insights for improving the understanding and prediction of woody debris flow behavior, particularly in post-wildfire landscapes.

Keywords: Inclined channel test, woody-debris suspensions, rheological properties, entry speed, deposit characteristics

1. INTRODUCTION

Debris flows, composed of water, soil, sand, rocks, and organic materials such as woody debris, are destructive and dynamic natural phenomenon prevalent in mountainous regions [1, 2]. In wildfire-affected forested areas, these flows pose significant threats to human life, infrastructure, and ecosystems. The presence of woody debris can further exacerbate their destructive potential by influencing flow mobility, deposition patterns, and overall flow behavior [2]. Woody debris is

believed to affect various aspects of debris flow behavior, including flow speed, flow depth, runout distance, and deposition [3]. While debris flow behavior has been widely studied, most research has primarily focused on sediment flows, with less attention given to the influence of organic material such as woody debris. Consequently, its effect on flow dynamics and rheological properties remain poorly understood, particularly in post-wildfire environments [4].

Woody debris interacts with the sediment-water mixture, alters its rheological properties, which are fundamental for predicting debris flow dynamics, designing mitigation strategies, and improving hazard assessment models [2, 5]. Previous studies on yield-stress fluids have shown that rigid inclusions or bubbles can modify rheology mainly through a crowding effect that increases the effective solid fraction, thereby enhancing yield stress and viscosity. At higher concentrations, direct contact between inclusions may promote frictional flow and particle migration [6, 7]. From this perspective, woody debris could behave as passive inclusions that increase the effective volume fraction, or as active elements whose elongated geometry, low density, and rough surfaces intensify frictional contacts and modify stress transmission and migration [1, 5, 8-10]. Understanding these interactions is particularly important because rheological characteristics directly control debris flow mobility [11-13]. However, conventional rheometers are typically limited to measuring fine-particle suspensions and cannot fully capture the influence of coarse particles or woody debris [14]. To overcome these limitations, indirect approaches for estimating rheological properties have been explored. For instance, the slump test has been used to infer rheological parameters based on correlations with slump and spread measurements [15]. Building on this framework, inclined channel tests commonly employed to investigate the flow behavior and runout characteristics of yield-stress fluid [10], offer a promising indirect method for characterizing debris flows with coarse and organic components. Specifically, Ancey & Jorrot [16] found that increasing sediment fraction in clay-water suspensions (with channel slopes of 15^{o} - 25^{o}) substantially raised yield stress and viscosity, reducing flow speed and producing thicker deposits due to enhanced particle interactions. Similarly, Coussot et al. [12] demonstrated that clay-based fluids with sediment concentrations exceeding 20% transition from fluid-like to solid-like behavior, with yield stress grows roughly with the square of the concentration. This transition leads to shorter runout distances and greater deposit thickness. These studies show that higher sediment concentrations strengthen yield-stress effects, constraining flow mobility, and promoting deposition. Such insights are particularly relevant to debris flows containing coarse particles or woody debris, for which inclined channel tests provide a robust framework to infer rheological properties.

This present study investigates how woody debris influences debris flow movement behavior and rheological characteristics in an inclined channel connected with a horizontal tank. Woody-debris suspensions with varying fine-sediment fractions, woody debris proportions, and woody debris sizes were used for both inclined channel tests and rheometer measurements. The woody debris used in the present study were pine sticks with a constant diameter of 6 mm and lengths of 10, 25, 40, and 55 mm, respectively. Through inclined channel tests, key flow parameters such as entry speed and deposit characteristics including runout distance, deposit width, deposit thickness, and final deposit profile in the horizontal tank, were measured and analyzed. Empirical equations were developed to relate entry speed to the fine-sediment fraction, woody debris proportion, and woody debris size using multiple linear regression analysis. The rheological characteristics of woody-debris suspensions were recorded using an ICAR rheometer, focusing on the effect of woody debris on rheological parameters, such as yield stress and viscosity. Furthermore, the

findings reveal significant correlations between rheological parameters (e.g., yield stress and viscosity) and inclined channel test parameters (e.g., entry speed, runout distance, and maximum deposit width). These results highlight the inclined channel test as a potential indirect method for estimating the rheological properties of debris flows containing woody debris.

2. MATERIALS - WOODY-DEBRIS SUSPENSIONS

In this study, woody-debris suspensions were prepared by mixing the fine-sediment suspensions, which contained fine-sediment fractions (C_{vf} = 0.25, 0.30, and 0.35) with the woody debris of varying proportions (C_{vg} = 0.00, 0.05, 0.10, 0.15, 0.20, and 0.25, respectively) and sizes (S_w = 10, 25, 40, and 55 mm, respectively), as shown in Table 1.

The fine-sediment suspensions consisted of highly concentrated clay-silt-water mixtures, with a sediment fraction of C_{vf}. A volume (V_f) of clay-silt was thoroughly mixed with tap water of volume (V_w) to form a fine-sediment suspension with a fine-sediment fraction (C_{vf}), as described by the equation:

$$C_{vf} = \frac{V_f}{V_f + V_w} \tag{1}$$

The clay-silt materials used in the experiments were collected from a reservoir deposition, washed multiple times, dried, and free of organic debris. These materials are consistent with those used in previous rheological studies by Jan & Dey [15] and Dey et al. [17], ensuring comparability with established research on fine-coarse particle suspensions. The clay component primarily comprises kaolinite, which is known to exhibit minimal thixotropic behavior compared to other clays such as bentonite [9]. The size distribution of the clay-silt materials is shown in Fig. 1a, with a medium diameter (D_{50}) of 0.0036 mm and a particle density of 2.65 g/cm^3 [24].

To prepare the woody-debris suspensions, a volume (V_g) of woody debris, consisting of pine sticks with a fixed diameter ϕ of 6 mm and lengths S_w of 10, 25, 40, and 55 mm (Fig. 1b), respectively was mixed with a volume (V_f+V_w) of fine-sediment suspension. These woody debris lengths correspond to aspect ratios ($AR = S_w/\phi$) of 1.67, 4.17, 6.67, and 9.17, and to bulk densities of 0.36, 0.32, 0.28, and 0.24 g/cm^3, respectively. This mixture formed a woody-debris suspension with a defined woody debris proportion (C_{vg}).

$$C_{vg} = \frac{V_g}{V_g + V_f + V_w} \tag{2}$$

A woody-debris suspension, containing fine sediment and woody debris, has a total sediment concentration of C_{vt}.

$$C_{vt} = \frac{V_f + V_g}{V_g + V_f + V_w} \tag{3}$$

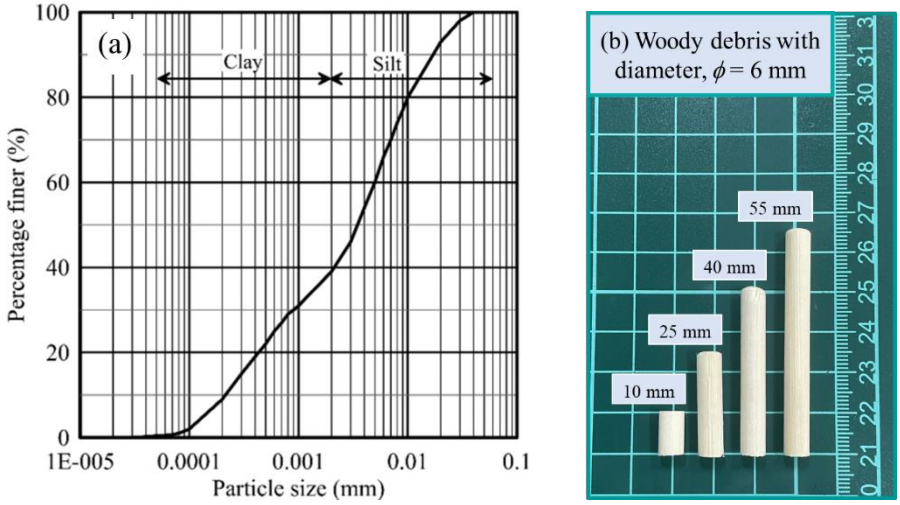

Fig. 1. (a) Size distribution of particles within the fine-sediment suspension and (b) woody debris attributes used in present experiments.

To illustrate the woody-debris suspensions used in the experiments, Fig. 2 presents a visual comparison of three representative samples (C25-1, C25-3, and C25-5), each with the same fine-sediment fraction (C_{vf} = 0.35) and woody debris size (S_w = 25 mm, corresponding to AR = 4.17), but different woody debris proportions (C_{vg}). These images highlight the woody debris distribution and overall mixture concentration as the C_{vg} varies, which in turn influences the rheological properties, flow behavior, and deposition characteristics.

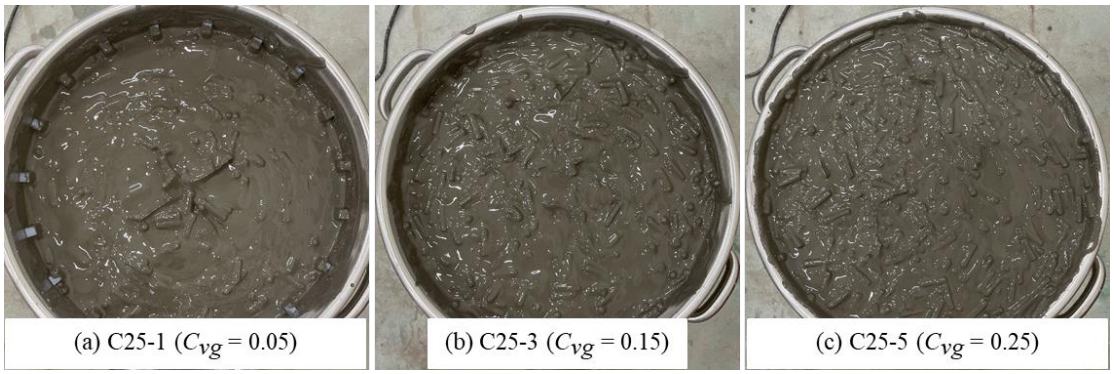

Fig. 2. Visual comparison of woody-debris suspensions C25-1, C25-3, and C25-5 with C_{vf} = 0.35 and S_w = 25 mm but varying C_{vg}

Table 1. Woody-debris suspensions and their corresponding sample numbers used in the present study.

Fine-sediment suspensions						
Fine-sediment fraction, C_{vf}		0.25		0.30		0.35
Sample number		A		B		C
Woody-debris suspensions with a base fine-sediment fraction, C_{vf} of 0.25						
Woody debris proportion, C_{vg}	0.00	0.05	0.10	0.15	0.20	0.25
Total sediment concentration, C_{vt}	0.25	0.29	0.33	0.36	0.40	0.44

Sample No. for various woody debris sizes, S_w (AR):						
10 mm (1.67)	A10-0	A10-1	A10-2	A10-3	A10-4	A10-5
25 mm (4.17)	A25-0	A25-1	A25-2	A25-3	A25-4	A25-5
40 mm (6.67)	A40-0	A40-1	A40-2	A40-3	A40-4	A40-5
55 mm (9.17)	A55-0	A55-1	A55-2	A55-3	A55-4	A55-5
Woody-debris suspensions with a base fine-sediment fraction, C_{vf} of 0.30						
Woody debris proportion, C_{vg}	0.00	0.05	0.10	0.15	0.20	0.25
Total sediment concentration, C_{vt}	0.30	0.34	0.37	0.41	0.44	0.48
Sample No. for various woody debris sizes, S_w (AR):						
10 mm (1.67)	B10-0	B10-1	B10-2	B10-3	B10-4	B10-5
25 mm (4.17)	B25-0	B25-1	B25-2	B25-3	B25-4	B25-5
40 mm (6.67)	B40-0	B40-1	B40-2	B40-3	B40-4	B40-5
55 mm (9.17)	B55-0	B55-1	B55-2	B55-3	B55-4	B55-5
Woody-debris suspensions with a base fine-sediment fraction, C_{vf} of 0.35						
Woody debris proportion, C_{vg}	0.00	0.05	0.10	0.15	0.20	0.25
Total sediment concentration, C_{vt}	0.35	0.38	0.42	0.45	0.48	0.51
Sample No. for various woody debris sizes, S_w (AR):						
10 mm (1.67)	C10-0	C10-1	C10-2	C10-3	C10-4	C10-5
25 mm (4.17)	C25-0	C25-1	C25-2	C25-3	C25-4	C25-5
40 mm (6.67)	C40-0	C40-1	C40-2	C40-3	C40-4	C40-5
55 mm (9.17)	C55-0	C55-1	C55-2	C55-3	C55-4	C55-5

3. EXPERIMENTAL STUDY

3.1. Inclined channel test

The experimental setup comprises two primary components: an inclined channel and a horizontal tank. The inclined channel, designed from transparent plexiglass, has 2 m in length, 0.1 m in width, and 0.2 m in height. A sliding gate at the upstream end serves as a suspension reservoir boundary (Fig. 3). At the lower end, the channel connects to a horizontal tank designed for suspension deposition, with dimensions of 1 m by 1 m. To facilitate accurate measurement and analysis of the deposit characteristics, the bottom of the horizontal tank is marked with a 1-cm grid.

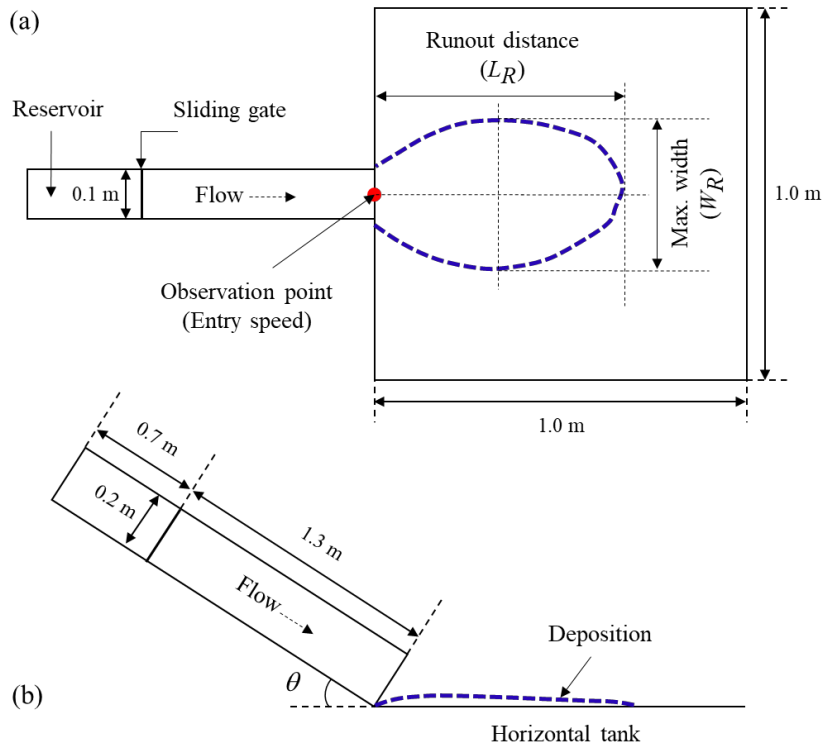

Fig. 3. Sketch showing of the laboratory installation, definitions, and measurements associated with the inclined channel test.

Each 2 liters of woody-debris suspension was released from a reservoir at the top of a 20° inclined channel by lifting a sliding gate. A slope of 20° was fixed for the tests as it reflects typical natural gradients where debris flows commonly initiate [2, 4], and is consistent with previous laboratory studies indicating that slopes between 15° and 25° are effective for simulating debris-flow behavior under controlled conditions [18]. The suspensions traveled 1.3 meters before entering and settling into a horizontal tank. To observe the movement and deposition, a top-view camera captured the images in the horizontal tank, while a side-view camera recorded the flow in the inclined channel. The recorded videos were later analyzed to calculate the entry speed of the debris flow. Once the suspension came to rest on the horizontal tank, the runout distance, deposit width, deposit thickness, and final deposit profile were measured using a laser distance meter. The runout distance was tracked by following the leading edge of the suspension flow (Fig. 3).

3.2. Rheological measurements using ICAR rheometer

Rheological measurements of complex yield-stress fluids, such as woody-debris suspensions, are crucial for advancing the understanding of debris flow behavior. Similar approaches have long been established in the field of fresh concrete rheology, where rotational rheometers are widely used to determine yield stress (τ_B) and plastic viscosity (μ_B) [19]. For instance, Jiao et al. [20] demonstrated that increasing aggregate content elevates yield stress by 20 - 40%, illustrating how coarse inclusions significantly enhance flow resistance. A comparable effect is observed in our suspensions, where the woody debris proportion (C_{vg}) markedly influences rheological properties. Unlike the relatively spherical or sub-angular aggregates in concrete, however, woody debris

exhibits anisotropic shapes and lower density, leading to unique challenges such as phase separation and enhanced inter-particle friction. To capture these complexities, this study employed an ICAR rheometer (Fig. 4), consisting of a large container, vane, and accompanying software, to reliably characterize the rheological properties of woody-debris suspensions. In detail, a container (RHM-3006) had a diameter of 355 mm and was filled with suspensions to a height of 380 mm. A four-bladed vane (RHM-3010), measuring 127 mm in both diameter and height, centrally positioned within the suspension, maintaining a 124-mm clearance above and below it (Fig. 4). The radius of the inner (R_i) and outer cylinders (R_o), were 63.5 mm and 177.5 mm, respectively, accommodating a maximum aggregate size of up to 25 mm. Additionally, outer cylinders are equipped with vertical strips to prevent slippage between the suspension and the steel surface.

Rheological measurements were conducted on woody-debris suspensions composed of clay, silt, and woody debris. However, phase separation could occur due to density differences, causing woody debris to rise and accumulate on the surface. This vertical segregation is exacerbated by shear-induced particle migration, a common phenomenon in suspension rheology where particles migrate from regions of high shear rate (near the vane or walls) to low shear rate areas due to gradients in shear rate, inter-particle interactions, and suspension viscosity, leading to inhomogeneous distributions and reduced measurement accuracy, particularly at low fine-sediment fractions [21-22]. In such cases, migration limits interaction with the rotating vane and can introduce apparent slip layers or diluted zones near shearing surfaces, distorting viscosity readings (Fig. 4) [22]. To mitigate these effects and ensure reliability, testing was limited to concentrated suspensions with $C_{vf} = 0.35$ and woody debris size of 25 mm ($AR = 4.17$), where the increased suspension viscosity and particle interactions minimize migration rates and vertical segregation, promoting a more homogeneous distribution [8].

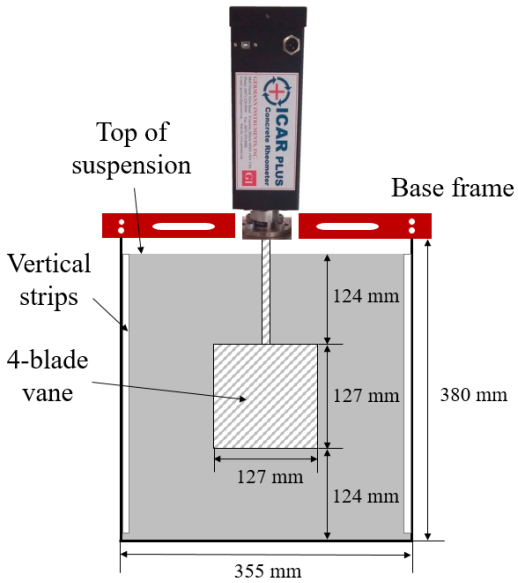

Fig. 4. Schematic diagram of rheological measurement by a ICAR rheometer.

Rheological measurements were performed using an ICAR rheometer equipped with a four-bladed vane (diameter $D = 127$ mm, height $h = 127$ mm) rotating in a large cylindrical cup (internal diameter 355 mm). The data were interpreted using the established localized-yielding assumption

for wide-gap vane geometries, in which yielding is confined to a thin sheared layer around the vane (effective radius ≈ $D/2$), while the surrounding material undergoes rigid-body rotation [9, 23, 24]. This provides the theoretical foundation for applying vane rheometry to pastes, suspensions, and debris-flow mixtures. Two types of tests were performed; in the stress growth tests, woody-debris suspensions were sheared at a constant rotational speed of 0.025 rev/s (corresponding to a shear rate of approximately 0.20 s^{-1}) for 60 seconds, and the static yield stress τ_0 was calculated from peak torque T_{max} using the standard vane expression accounting for shear on both the cylindrical surface and end faces [9, 24]:

$$\tau_0 = T_{max}\left(\frac{2}{\pi D^2}\right)\left(\frac{1}{h}+\frac{1}{3D}\right) \tag{4}$$

During these tests, the shear stress stabilized after reaching its peak value, with no significant time-dependent reduction, confirming that the kaolinite-based fine-sediment suspension is non-thixotropic and that the flow reached a steady state. On the other hand, the flow curve tests for woody-debris suspensions were conducted to determine Bingham parameters (yield stress and viscosity), using a breakdown time of 20 s, a rotational speed range from 0.05 to 0.65 rev/s, 13 measurement points, and 5 seconds per point. Eq. 5 was used to plot flow curves in relative units based on the best-fit line for each suspension:

$$T = G + HN \tag{5}$$

where T is the torque (Nm), G is the intercept (Nm) linked to Bingham yield stress τ_B, H is the slope (Nm.s) linked to Bingham viscosity μ_B, and N is the rotational speed (rev/s) [25], as shown in Eq. 6:

$$\tau = \tau_B + \mu_B\dot{\gamma} \tag{6}$$

where, τ is shear stress (Pa), τ_B is Bingham yield stress (Pa), μ_B is Bingham viscosity (Pa.s), and $\dot{\gamma}$ is shear rate (s^{-1}). Güneyisi et al. [26] provided an equation that enables the conversion of rotational speed (N) and torque (T) into key rheological parameters, shear stress (τ) and shear rate ($\dot{\gamma}$) using the manufacturer-supplied conversion constants, as shown below:

$$\tau = \frac{(R_i^2 + R_o^2)}{4\pi h R_i^2 R_o^2}\,T \tag{7}$$

$$\dot{\gamma} = \frac{(R_i^2 + R_o^2)}{(R_o^2 - R_i^2)}\,N \tag{8}$$

These constants are derived from Newtonian calibration and implicitly incorporate the localized-yielding assumption together with end effects for the specific ICAR vane-cup geometry. Their use is well established for yield stress debris-flow materials containing large particles [27].

4. RESULTS AND DISCUSSIONS

4.1. Flow behavior of woody-debris suspensions

Woody-debris suspensions flowing down a 20° inclined channel and settling on a horizontal tank exhibit three main stages: first, the initial release and mobilization of the material; second, its transport along a 1.3-meter inclined channel; and third, the eventual deposition on the horizontal tank. The experiment also involved measuring the entry speed (V_0) at the observation point, the intersection of supensions at the downstream of the inclined channel before the horizontal tank, as shown in Fig. 3a. The characteristics and deposition patterns of the final deposits are influenced by the fine-sediment fraction (C_{vf}), woody debris proportion (C_{vg}), and woody debris size (S_w).

In this study, the value of V_0 was determined from video recordings by measuring the runout length (ΔL) downstream of the inclined channel over time (Δt), expressed as $V_0 = \Delta L / \Delta t$ [28]. This parameter presents the speed at which sediment suspensions enter the horizontal tank. The influence of C_{vf}, C_{vg}, and S_w on the V_0 was investigated for woody-debris suspensions under an inclined channel θ of 20^o (Fig. 5). As illustrated in Fig. 5, the V_0 exhibits a systematic decrease with increasing C_{vf} and C_{vg}. A slight increase in V_0 is observed with larger S_w. This highlights the critical influence of fine-sediment fraction, woody debris proportion, and woody debris size on flow mobility and rheology. Specifically, a decrease in C_{vf} leads to reduced cohesion within the suspension, lowering its yield strength and allowing for faster initial acceleration. This is consistent with the established understanding that fine particles contribute to the cohesive properties of fluid-suspension mixtures. Similarly, a lower C_{vg} minimizes internal resistance and obstruction within the flow, promoting smoother and more rapid movement. In contrast, an increase in S_w enhances V_0, as larger particles reduce inter-particle crowding and frictional contacts, while size-driven segregation further lowers resistance and facilitates faster downslope motion [16]. As a result, the sediment suspension moves faster and travels further [1]. However, field observations show that larger S_w often reduces V_0 due to entrainment and jamming, driven by increased mechanical resistance and form drag from larger, denser elements [1, 13, 29]. In our laboratory setup, the minimization of large-scale jamming, unlike in natural terrains, allows the rheological influence of coarser fractions to prevail, resulting in higher entry speeds and longer runout distances [30].

Furthermore, the experimental results revealed that the C_{vf} had a stronger influence on the V_0 than either the C_{vg} or S_w (Fig. 5). This aligns with the findings of Ancey & Jorrot [16], who demonstrated that in sediment suspensions containing both fine and coarse particles, the rheological behavior is primarily governed by the fine-particle fraction, provided that its proportion exceeds that of the coarse particles. This suggests that in our experiments, the C_{vf} played a dominant role in controlling flow behavior, particularly when its proportion was greater than that of woody debris. The interplay between these factors highlights the complexity of woody-debris suspension dynamics and the need to consider both sediment composition and woody debris characteristics when analyzing flow behavior.

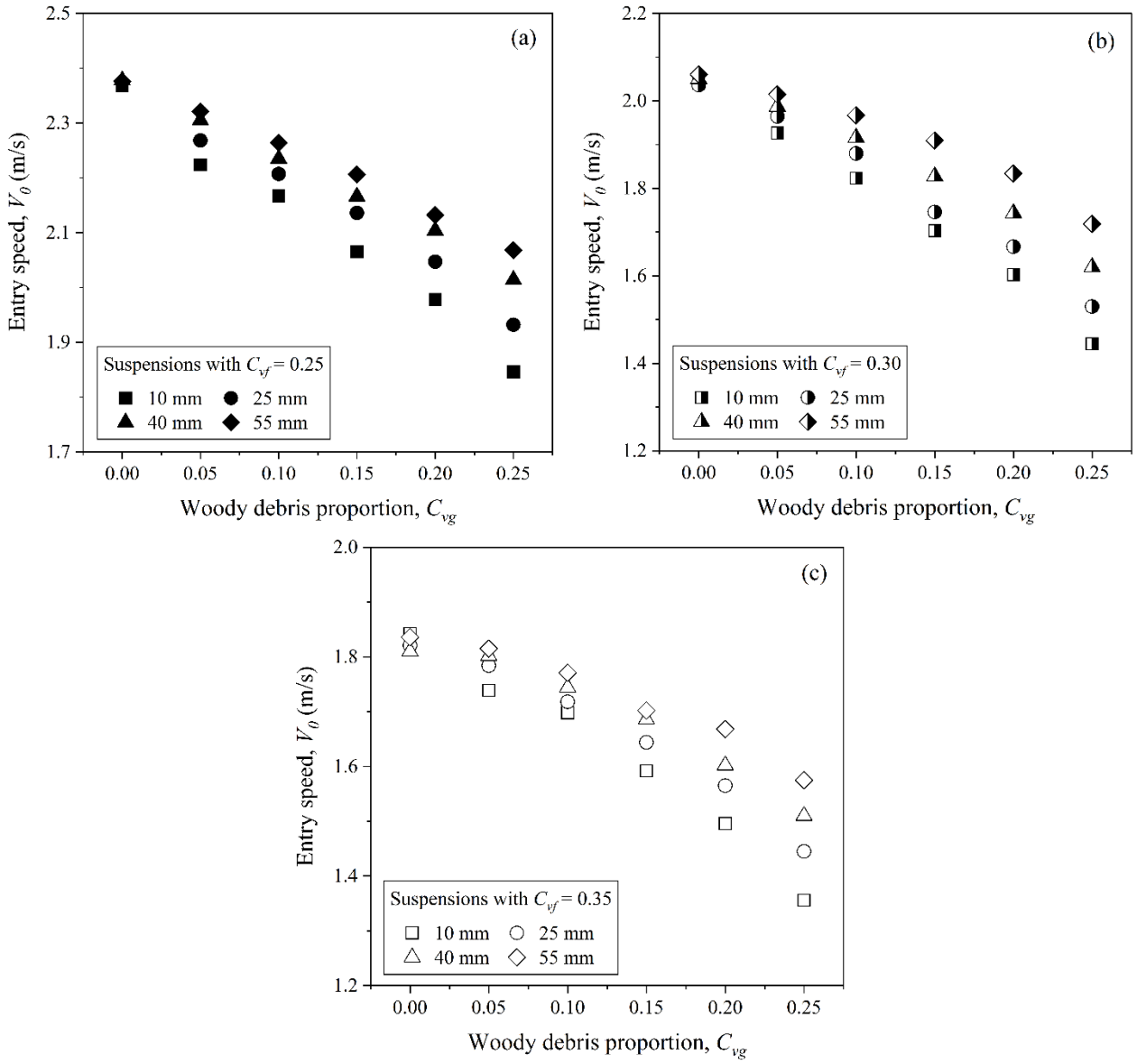

Fig. 5. The entry speed V_0 for the tests under different fine-sediment fraction C_{vf}, woody debris proportion C_{vg}, and woody debris size S_w of woody-debris suspensions at channel slopes θ of 20°.

As shown in Fig. 5, the V_0 of woody-debris suspensions at a channel slope of 20° are strongly related to the C_{vf}, C_{vg}, and S_w. This relationship can be expressed by the following equation:

$$V_0 = a_1 C_{vf} + b_1 C_{vg} + c_1 S_w + d_1 \tag{9}$$

Through a multiple linear regression analysis, the fitting coefficients a_1, b_1, c_1, and d_1 for the present experimental conditions of $0.25 \le C_{vf} \le 0.35$, $0 \le C_{vg} \le 0.25$, and $10 \le S_w \le 55$ mm at a 20° channel slope were found to be -5.28, -1.75, 2.68, and 3.61, respectively where V_0 in m/s and S_w in m. The obtained coefficients further reinforce that the C_{vf} has a more pronounced influence compared to C_{vg} and S_w. Figure 6 presents a comparison between the experimentally measured V_0 of different woody-debris suspensions and the V_0 calculated using Eq. 9. The experimental data

closely follow a line that passes through the origin. With a coefficient of determination ($R^2 = 0.96$), the results suggest that Eq. 9 provides a fairly accurate method for predicting V_0 based on the C_{vf}, C_{vg}, and S_w at a channel slope of 20^o. Since entry speed is a crucial factor influencing the subsequent dynamics and deposition of debris flows, this predictive equation is valuable for both understanding and modeling these phenomena.

To further enhance the understanding of yield-stress fluid behavior in channels with different debris-flow materials, we collected measured V_0 for various sediment suspensions from Chang et al. [31] and Wang et al. [32], as summarized in Table 2. These studies examined materials with fine-sediment fractions ($C_{vf} = 0.25$ - 0.40), large-particle fractions ($C_{vg} = 0.15$ - 0.30), and large-particle sizes (S_w up to 100 mm). Using Eq. 9, we calculated the V_0 for these samples and compared them with our experimental results. The comparison in Fig. 6 confirms that Eq. 9 reliably predicts V_0 for a wide range of debris-flow materials. Notably, Chang et al. [31] and Wang et al. [32] observed results consistent with ours showing that higher C_{vg} increases τ_B and μ_B, leading to reduced V_0 due to the enhanced structural resistance provided by the woody debris matrix (S_w = 25 mm). Conversely, lower C_{vf} (0.25, 0.30) or smaller S_w reduces τ_B by decreasing frictional interactions, thereby increasing V_0 [1]. Steeper channel slopes amplify the gravitational driving force, further increasing V_0, consistent with observations in debris flow studies [2].

Table 2. Properties of suspension samples and corresponding entry speeds (from literature).

Reference	θ (^{o})	C_{vf}	C_{vg}	S_w (mm)	Measured V_0 (m/s)	Calculated (Eq. 9) V_0 (m/s)
Chang et al. [31]	20	0.25	0.15	9.5	2.27	2.28
	20	0.30	0.15	9.5	2.08	2.02
	20	0.30	0.20	9.5	1.91	1.93
	20	0.35	0.20	9.5	1.81	1.67
	20	0.35	0.25	9.5	1.63	1.58
Wang et al. [32]	8.53	0.40	0.30	100	0.98	1.01

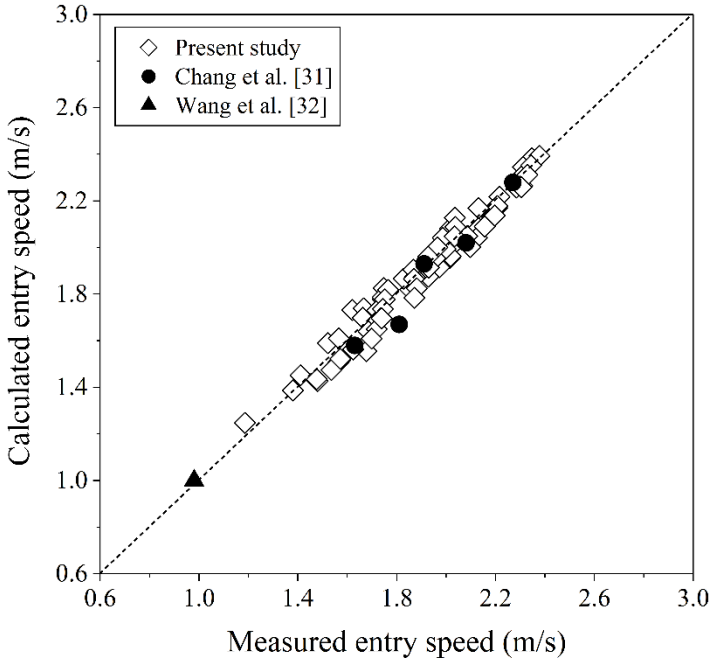

Fig. 6. The measured entry speeds compared with the calculated entry speeds for woody-debris suspensions with varying fine-sediment fractions, woody debris proportions, and woody debris sizes at channel slopes of 20°.

4.2. Deposit characteristics

This section presents the results of experiments that investigate the influence of fine-sediment fractions (C_{vf}), woody debris proportions (C_{vg}), and woody debris sizes (S_w) on key deposit characteristics, including runout distance (L_R), deposit width (W_R), deposit thickness (H_R), and final deposit profile.

4.2.1. Effect of fine-sediment fraction, C_{vf}

Figure 7 shows the final deposit profiles, including both longitudinal cross-sections and top-views, were analyzed to estimate the behavior of woody-debris suspensions. These deposits were formed as suspension flowed down an inclined channel at a slope θ of 20° and settled in a horizontal tank. As illustrated in Fig. 7a, the longitudinal cross-sectional profiles reveal how varying C_{vf} (0.25 - 0.35) influence deposit characteristics while keeping the C_{vg} = 0.15 and S_w = 55 mm constant. A lower C_{vf} produces thinner deposits that gradually diminish along the runout distance. In contrast, a higher C_{vf} results in thicker deposits, particularly at the front, where woody debris tends to accumulate. Figure 7b displays the top-view profiles, highlighting differences in deposit width evolution. Initially, the deposit expands in width before gradually narrowing as suspension propagates further. Lower C_{vf} form narrower deposits with longer runout distances, whereas those with higher C_{vf} exhibit progressively wider deposits and shorter runout distances. These results are consistent with previous findings on the influence of woody debris on runout distance, deposit width, and morphology, as presented by Takahashi [2].

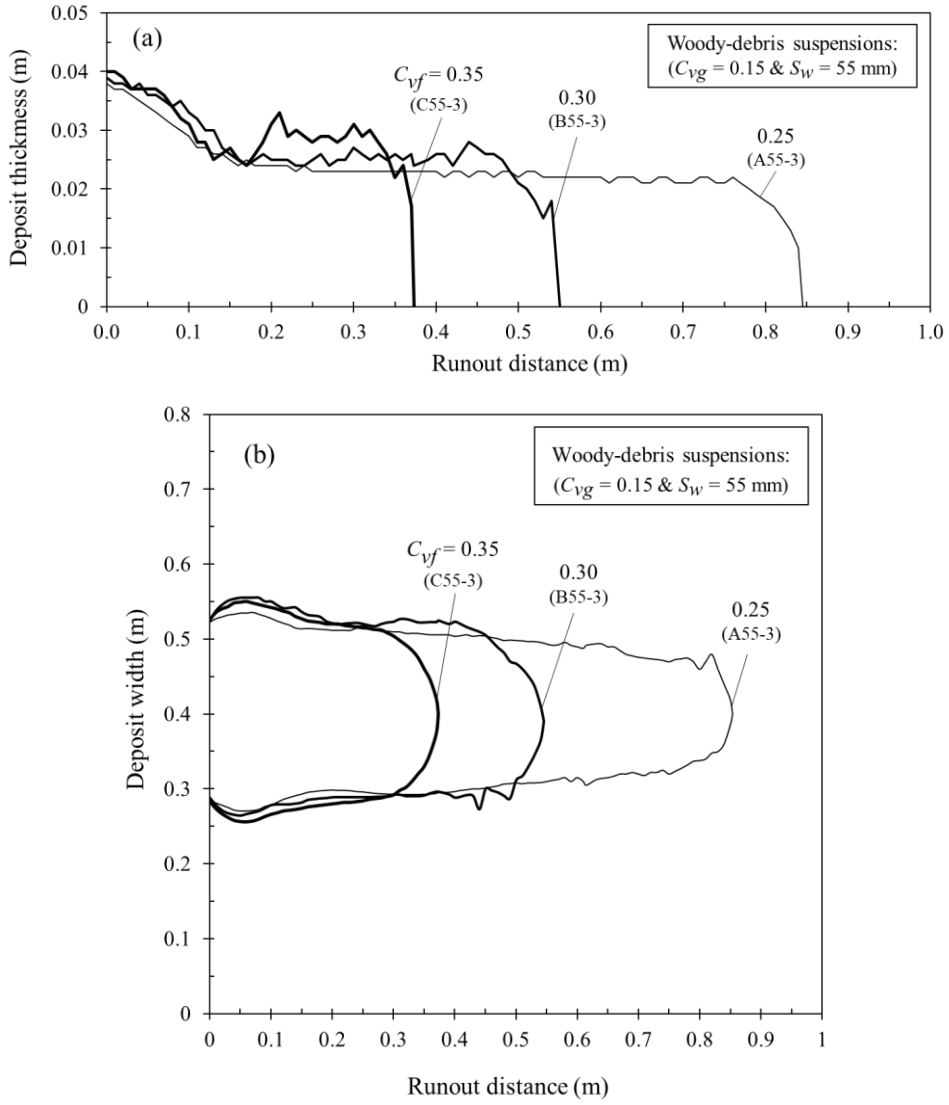

Fig. 7. Final deposit profiles: (a) longitudinal cross-sectional profiles and (b) top-view of deposits for tests under $\theta = 20^{o}$ for woody-debris suspensions with same $C_{vg} = 0.15$ and $S_w = 55$ mm but different C_{vf}.

4.2.2. Effect of woody debris proportion, C_{vg}

The influence of C_{vg} (0 - 0.25) on deposit morphology is depicted in Fig. 8. The longitudinal cross-sectional profiles (Fig. 8a) illustrate results for suspensions with a fixed $C_{vf} = 0.30$ and $S_w =$ 55 mm, while varying C_{vg}. A lower C_{vg} results in thinner deposits with a gradual decline along the runout distance. Conversely, as C_{vg} increases, the deposits become noticeably thicker, maintaining their structure over a greater portion of the runout distance. Figure 8b further explores the effect of C_{vg} on deposit shape from a top-view perspective, showing an initial increase in deposit width, followed by a gradual decrease as the suspension progresses further into the horizontal tank. Suspensions with lower C_{vg} exhibit narrower deposit widths and longer runout distances, whereas those with higher C_{vg} display progressively wider deposit widths and shorter runout distances. This observation can be attributed to the woody debris, which increases the total sediment

concentration of the mixture (elevating C_{vg}), but more critically, induces mechanical resistance through jamming and interlocking effects at the flow front. These processes enhance basal friction and diffusivity, outweighing any temporary reduction in effective friction from elevated pore pressures, thereby decreasing flow speed and runout distance [17, 29]. These findings align with previous studies on the effects of woody debris on runout distance and overall deposit morphology, as reported by Lancaster et al. [13] and Rengers et al. [33].

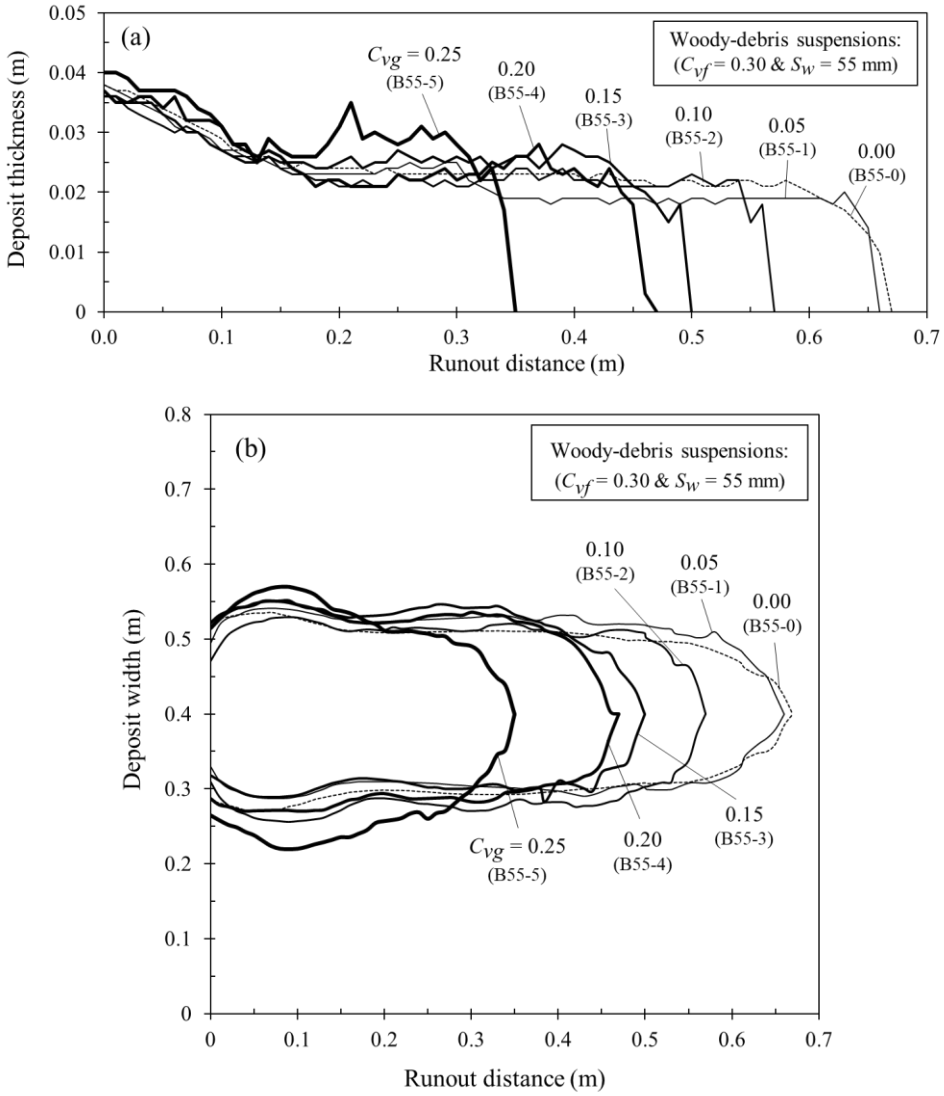

Fig. 8. Final deposit profiles: (a) longitudinal cross-sectional profiles and (b) top-view of deposits for tests under $\theta = 20^{o}$ for woody-debris suspensions with same $C_{vf} = 0.30$ and $S_w = 55$ mm but different C_{vg}.

4.2.3. Effect of woody debris size, S_w (AR)

Figure 9 provides insights into how woody debris size influences final deposit characteristics. The longitudinal cross-sections in Fig. 9a correspond to the woody-debris suspensions with a constant $C_{vf} = 0.30$ and $C_{vg} = 0.20$, while S_w varies from10 to 55 mm (AR = 1.67 - 9.17). The results show that larger S_w (AR) leads to thinner deposits, whereas smaller S_w (AR) contributes to

thicker deposits with a more gradual reduction in thickness along the runout distance. Examining the top-view deposit profiles in Fig. 9b, a clear distinction emerges in the spatial distribution of deposits. Suspensions with smaller S_w (AR) exhibit wider, more laterally spread deposits, while those with larger S_w (AR) tend to form narrower deposits with greater runout distances. These findings align with Matioli et al. [34], which similarly reported a strong relation of woody debris size to the flow width and runout distance.

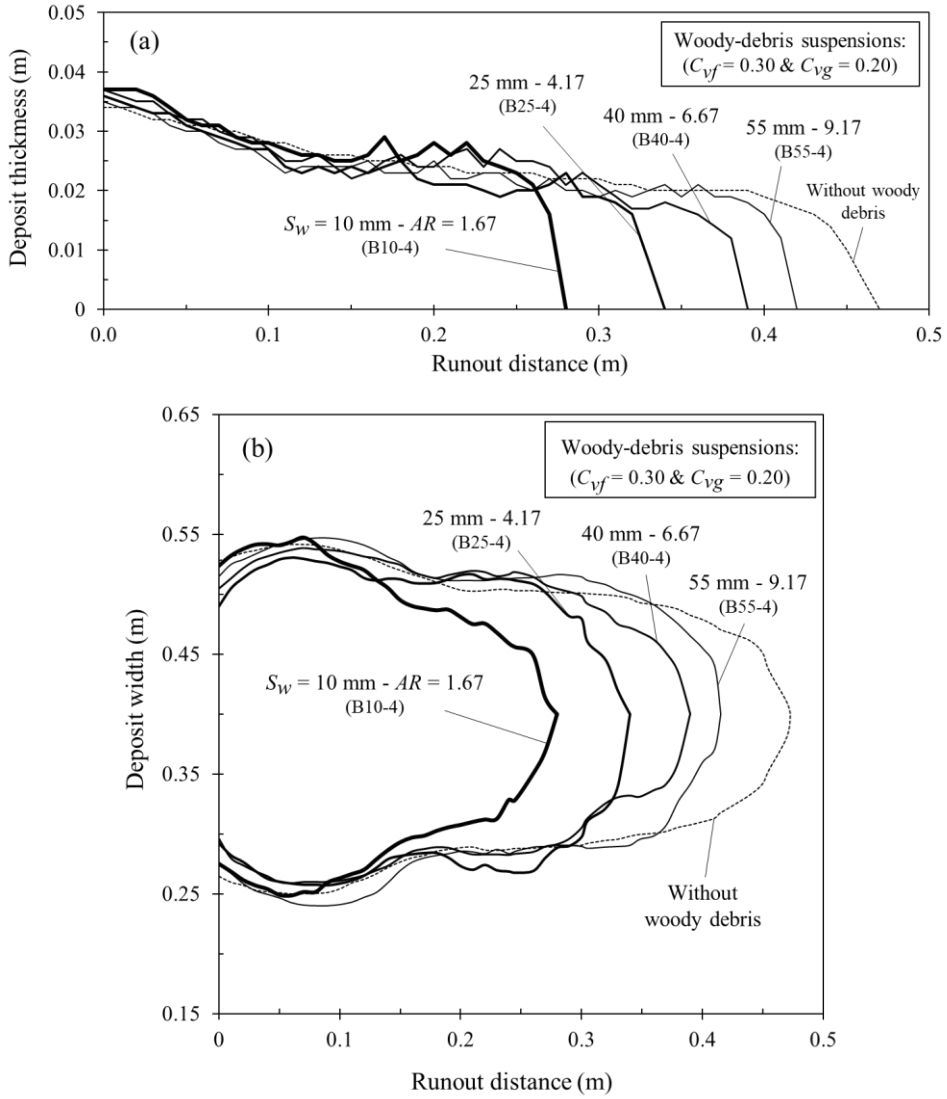

Fig. 9. Final deposit profiles: (a) longitudinal cross-sectional profiles and (b) top-view of deposits for tests under $\theta = 20^{o}$ for woody-debris suspensions with same $C_{vf} = 0.30$ and $C_{vg} = 0.20$ but different S_w (AR).

Overall, the results show that increasing the fine-sediment fraction and woody debris proportion lowers entry speeds, leading to shorter runout distances, thicker deposits, and wider extents. In contrast, larger woody debris sizes enhance entry speeds, resulting in longer runout distances while producing thinner and narrower deposits. Among the analyzed deposit characteristics, runout distance exhibited greater sensitivity to variations in deposit width and

thickness. This suggests that even minor changes in these parameters can substantially impact the extent of flow propagation. Furthermore, observations and final deposit profiles of woody-debris suspensions indicate that woody debris tends to accumulate at the front during movement and deposition [35, 36]. As a result, variations in deposit thickness, governed by material conditions are primiraly pronounced at the front of deposits (Figs. 7a, 8a, and 9a).

4.3. Correlations between entry speeds and deposit characteristics

Investigating the relationship between entry speed (V_0) and deposit characteristics, such as runout distance (L_R) and maximum deposit width (W_R), is crucial for understanding debris flow dynamics and deposition mechanisms in inclined channel tests. Figure 10 illustrates the correlation between V_0 and L_R for woody-debris suspensions with varying C_{vf}, C_{vg}, and S_w. The results reveal a positive correlation, where higher V_0 correspond to greater L_R. This observed trend aligns with findings from Iverson et al. [4]. To better capture the influence of C_{vf}, the relationship between V_0 and L_R was further evaluated separately for each tested value of C_{vf} (0.25, 0.30, 0.35), corresponding to Eqs. 10, (11), and (12), respectively. These empirical relationships, established under varying conditions of C_{vg} and S_w, are expressed as power-law functions depending on the value of C_{vf}.

$$L_R = a_2 V_0^{b_2} \tag{10}$$

$$L_R = a_3 V_0^{b_3} \tag{11}$$

$$L_R = a_4 V_0^{b_4} \tag{12}$$

The fitting parameters (a_2, b_2), (a_3, b_3), and (a_4, b_4) obtained from experimental data are (0.11, 2.64), (0.15, 2.07), and (0.14, 1.87), respectively, where V_0 is measured in m/s and L_R in m. A noticeable decrease in the exponents b_2, b_3, and b_4 with the reduction of C_{vf} highlights the significant influence of C_{vf} on both the V_0 and the L_R observed in this study. Furthermore, the relationship between V_0 and L_R, as described in Eqs. 10, (11), and (12), is characterized by the exponents $b_2 = 2.64$, $b_3 = 2.07$, and $b_4 = 1.87$, all of which are significantly greater than 1.0. This indicates a strong dependence of the L_R on the V_0 of woody-debris suspensions. Notably, even a slight increase in V_0 can result in a significant extension of the L_R. These findings underscore the critical role of entry speed in governing the final runout distance and deposit morphology, offering valuable insights for predictive modeling and the broader understanding of debris flow dynamics.

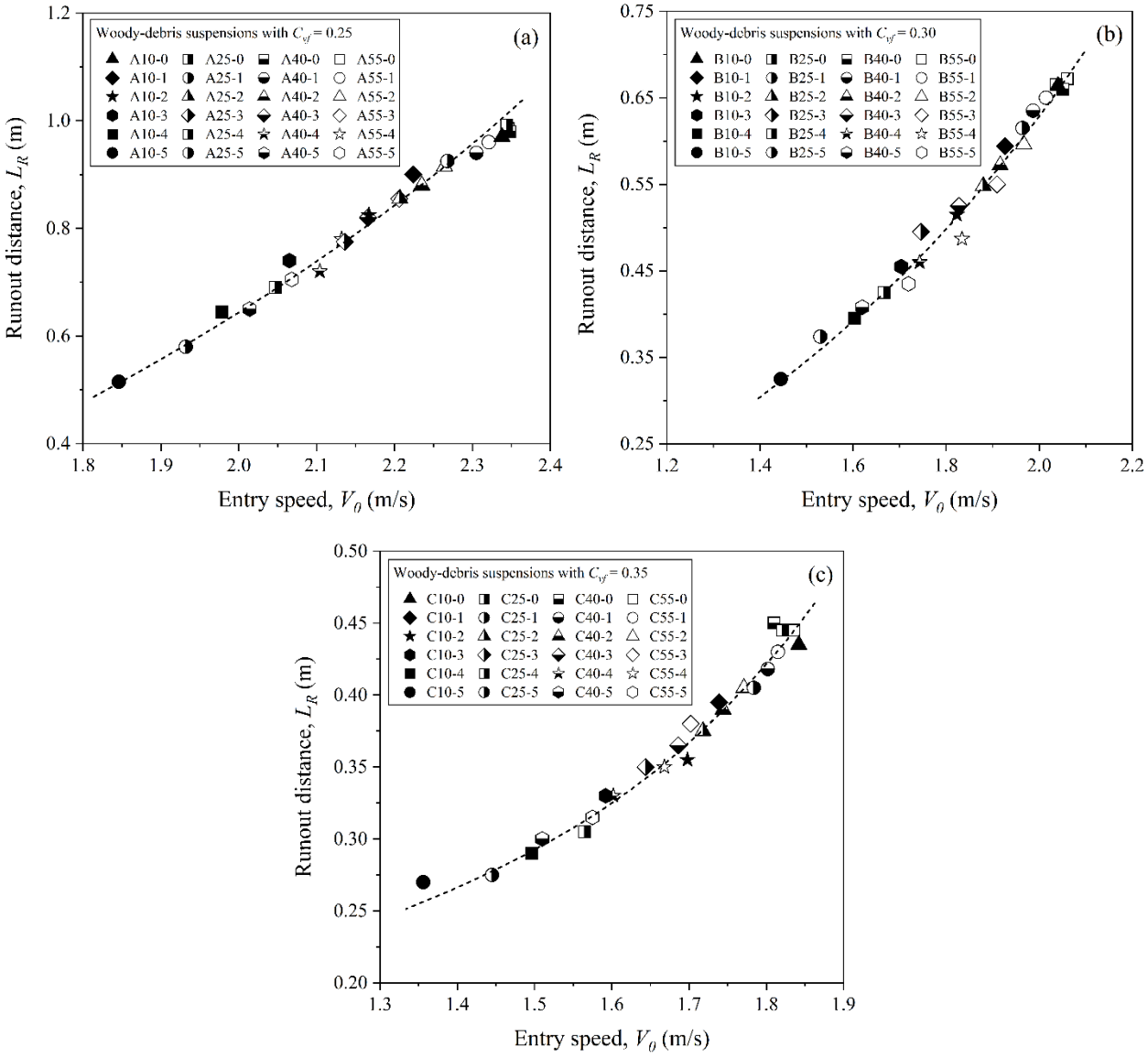

Fig. 10. The runout distance L_R related to entry speed V_0 for varying C_{vf}, C_{vg}, and S_w of woody-debris suspensions at channel slopes of 20°.

Figure 11 illustrates the relationship between entry speed (V_0) and maximum deposit width (W_R) of the final deposits for the various tested woody-debris suspensions. The results indicate a negative correlation between V_0 and W_R, where an increase in V_0 is associated with a decrease in W_R. These inverse relationships are expressed mathematically for each tested value of the fine-sediment fraction (C_{vf}) as follows:

$$W_R = a_5 - b_5 V_0^{c5} \quad (13)$$

$$W_R = a_6 - b_6 V_0^{c6} \quad (14)$$

$$W_R = a_7 - b_7 V_0^{c7} \quad (15)$$

For suspensions tested under varying C_{vg} and S_w, the fitted coefficient sets (a_5, b_5, c_5), (a_6, b_6, c_6), and (a_7, b_7, c_7), corresponding to C_{vf} (0.25, 0.30, 0.35), were found to be (0.48, 0.02, 2.81), (0.45, 0.02, 3.31), and (0.48, 0.01, 4.15), respectively. In these models, V_0 expressed in m/s and W_R in m. Overall, the empirical equations presented in Eqs. 10-15 emphasize the considerable impact of the entry speed on the final characteristics of the deposit, particularly the runout distance and maximum deposit width. Although the results are specific to the experimental setup and materials, they provide useful insights for predictive models and a deeper understanding of debris flow behavior.

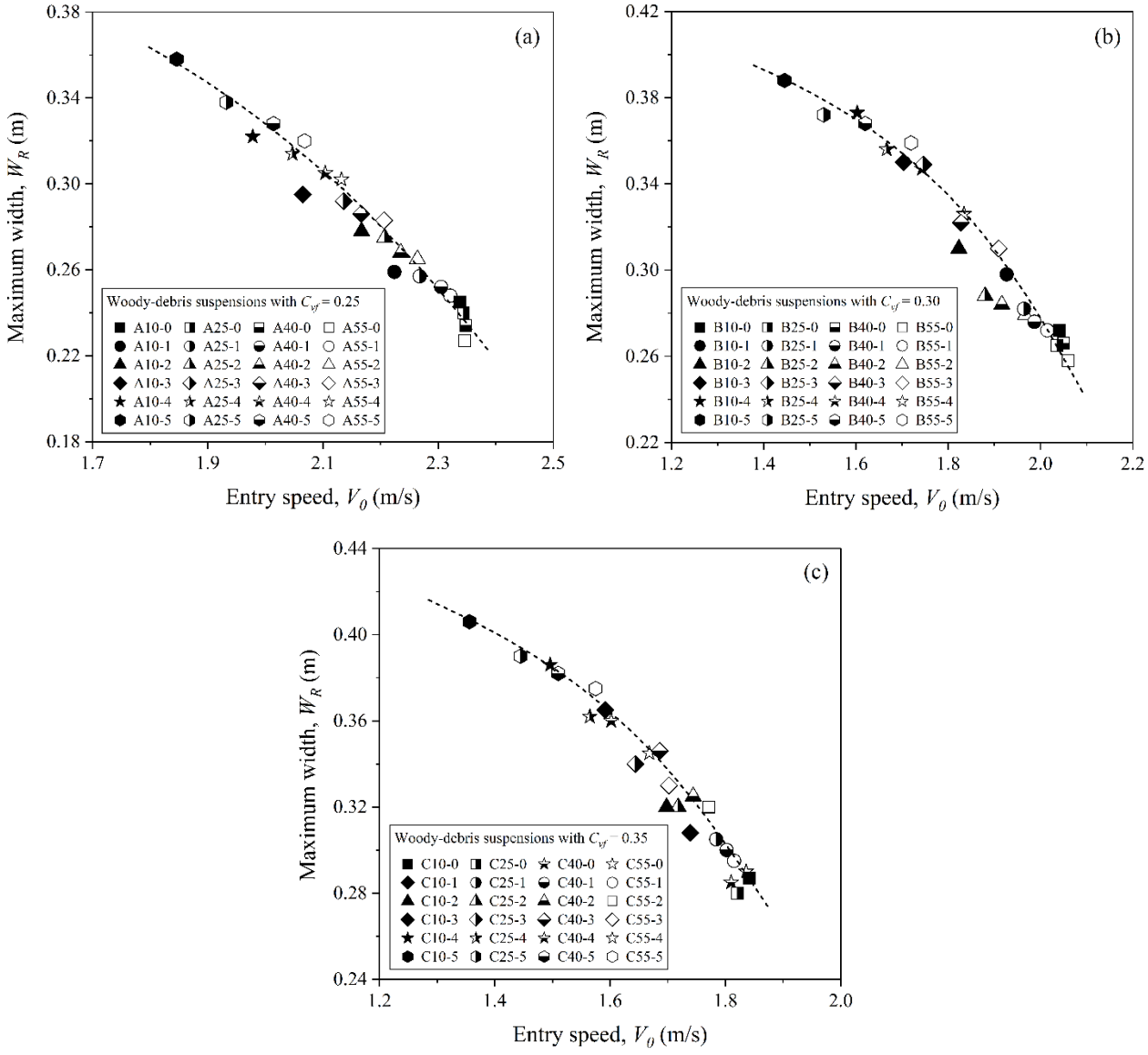

Fig. 11. The maximum deposit width W_R related to entry speed V_0 for varying C_{vf}, C_{vg}, and S_w of woody-debris suspensions at channel slopes of 20°.

4.4. Rheological properties of woody-debris suspensions

The rheological behavior of debris flow material arises from complex interactions between fluid viscosity, particle friction, and collisions, influenced by shear rate, sediment fraction, particle size, and sediment distribution [17]. In this study, the rheological properties of woody-debris suspensions were measured using an ICAR rheometer. Regarding the control of vertical segregation in woody debris, rheological measurements were performed on woody-debris suspensions with fine-sediment fraction (C_{vf} = 0.35) and woody debris size (S_w = 25 mm), while varying woody debris proportion (C_{vg}). The suspensions showed a steady and homogeneous response, confirmed by stress growth tests, which revealed no significant time-dependent stress reduction, and by hysteresis tests, where torque-speed curves nearly overlapped during increasing and decreasing rotational speeds. These results indicate that the woody-debris suspensions achieved steady-state flow and the rheological measurements are reliable and reproducible.

Figure 12 shows a linear correlation between torque (T) and rotational speed (N), which can be converted into shear stress (τ) and shear rate ($\dot{\gamma}$) using Eqs. 7 and (8). For woody-debris suspensions with a fine-sediment fraction of C_{vf} = 0.35, the rotational speed ranged from 0.05 to 0.65 rev/s, producing to torque values between 0.20 and 0.48 Nm. These values convert to a shear rate of 0.40 to 5.30 s^{-1} and a shear stress ranging from 62.5 to 149.2 Pa. The flow curves in Fig. 12, consistent with field shear rates below 10 s^{-1} [37], reveal distinct rheological behavior described by the Herschel-Bulkley model with power-law index n. Specifically, at low shear rates, the suspensions exhibit shear-thinning behavior (n < 1), characterized by a non-linear increase in shear stress that initially rises and then decreases, due to reduced viscosity from particle network breakdown or woody debris realignment, with fluid viscosity dominant. In contrast, at higher shear rates, a linear trend in shear stress emerges, which can be approximated by a Bingham fluid model (n = 1) as described in Eq. 6, consistent with findings of Ancey & Jorrot [16] and Dey et al. [17].

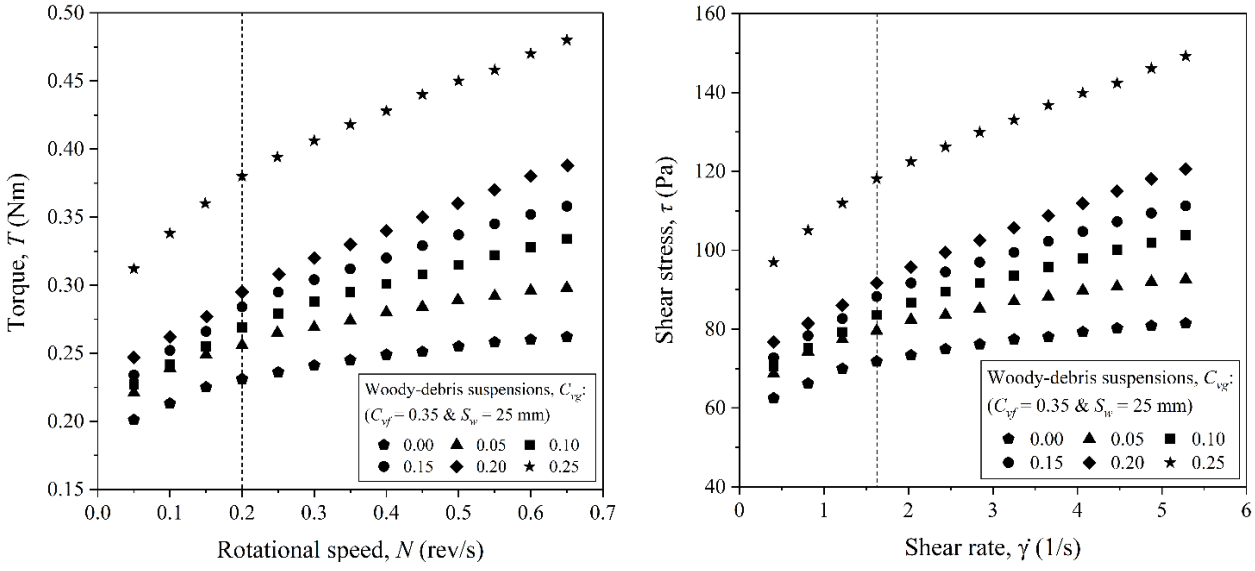

Fig. 12. Rheological relations of woody-debris suspensions with the same C_{vf} of 0.35 and S_w of 25 mm but different C_{vg}.

The influence of woody-debris volume fraction on the rheology is presented in dimensionless form in Fig. 13 and Table 3. Both the Bingham yield stress and viscosity increase markedly with increasing woody debris proportion. As shown in Fig. 13a, the relative yield stress (τ_B/τ_{B0}), collapses onto a single master curve when plotted against the reduced volume fraction $C_{vg}/C_{vg\text{-}max}$ using a maximum packing fraction $C_{vg\text{-}max} \approx 0.58$. This collapse aligns closely with literature data for suspensions of spherical beads in yield-stress matrices, which typically exhibit $C_{vg\text{-}max} \approx 0.62$ - 0.64 [17, 38, 39], indicating that yield-stress reinforcement in woody-debris suspensions is governed by a universal, largely shape-independent jamming mechanism. Figure 13b presents the relative viscosity (μ_B/μ_{B0}), of the same suspensions. The data are compared with the theoretical predictions of Chateau et al. [6] for non-colloidal inclusions suspended in a Herschel-Bulkley matrix of flow-behavior index n, using the same $C_{vg\text{-}max} \approx 0.58$. The experimental points fall between the Bingham-matrix bound (n = 1) and the strongly shear-thinning bound (n = 0.5), but increase markedly faster than the Bingham prediction. This stronger viscosity enhancement highlights the important contributions of particle anisotropy, surface friction, and mechanical interlocking of the elongated woody debris. Overall, while the yield stress follows a universal jamming-controlled scaling similar to spherical-particle systems, the plastic viscosity is substantially amplified by the elongated shape and frictional interactions of the woody elements.

Table 3. Comparison of suspensions and their parameters reported by different researchers.

Reference	Suspension	C_{vg}	$C_{vg}/C_{vg\text{-}max}$	τ_B/τ_{B0}	μ_B/μ_{B0}
Present study	Fine-sediment slurry + woody debris	0	0	1.00	1.00
		0.05	0.09	1.06	1.17
		0.10	0.17	1.09	1.69
		0.15	0.26	1.18	1.95
		0.20	0.35	1.29	2.21
		0.25	0.43	1.54	2.90
Dey et al. [17]	Fine-sediment slurry + spherical glass beads	0	0	1.00	-
		0.15	0.26	1.25	-
		0.20	0.35	1.42	-
		0.25	0.43	1.60	-
		0.30	0.52	1.79	-
Mahaut et al. [38]	Dense emulsions + spherical glass beads	0	0	1.00	-
		0.15	0.26	1.06	-
		0.30	0.52	1.30	-
		0.40	0.69	1.96	-
		0.45	0.78	2.81	-
Ovarlez et al. [39]	Emulsions + spherical beads	0	0	1.00	-
		0.20	0.35	1.65	-
		0.35	0.60	2.86	-
		0.50	0.86	6.05	-

Note: τ_{B0} and μ_{B0} values for the pure suspending fluid (C_{vg} = 0): Present study = 69.20 Pa, 0.42 Pa.s; Dey et al. = 11.58 Pa; Mahaut et al. [38] = 39.84 Pa; Ovarlez et al. [39] = 9.85 Pa.

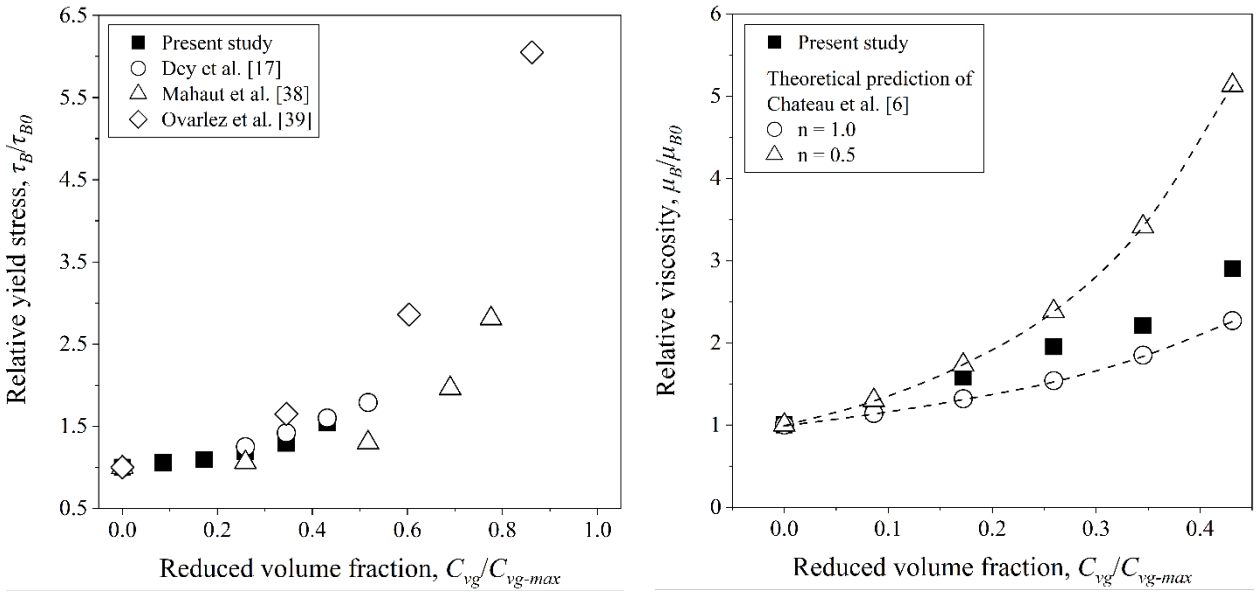

Fig. 13. Scaling of (a) relative yield stress τ_B/τ_{B0} and (b) relative viscosity μ_B/μ_{B0} with reduced woody-debris volume fraction $C_{vg}/C_{vg\text{-}max}$.

4.5. Correlations between the rheological parameters and inclined channel test parameters

During the inclined channel test, woody-debris suspensions flow down an inclined plane under the influence of gravity, mimicking natural debris flow dynamics. As the suspension begins to flow, its movement is governed by the applied shear stress generated by the gravitational force acting along the slope. The flow continues until the shear stress drops below the yield stress of the suspension, at which point the flow ceases, and deposition occurs on the horizontal tank. This process highlights a direct relationship between the flow behavior and rheological properties, such as yield stress, shear stress, viscosity, and shear rate.

In this study, the rheological parameters (e.g., yield stress and viscosity) obtained from rheometer measurements were systematically compared with flow parameters (e.g., entry speed), and deposit parameters (e.g., runout distance and maximum deposit width) from inclined channel tests. These relationships are illustrated in Fig. 14. The analysis revealed strong linear correlations, with coefficients of determination (R^2) ranging from 0.81 to 0.98 (Table 4). As noted by Cohen et al. [40], R^2 values greater than 0.7 are typically considered strong, confirming a significant relationship between rheological properties and flow behaviors. Notably, the correlations involving entry speed and runout distance exhibited stronger relationships with rheological parameters than those involving maximum deposit width. These findings suggest that entry speed and runout distance, as obtained from inclined channel tests, may serve as viable indirect methods for estimating the rheological parameters of debris flows containing woody debris.

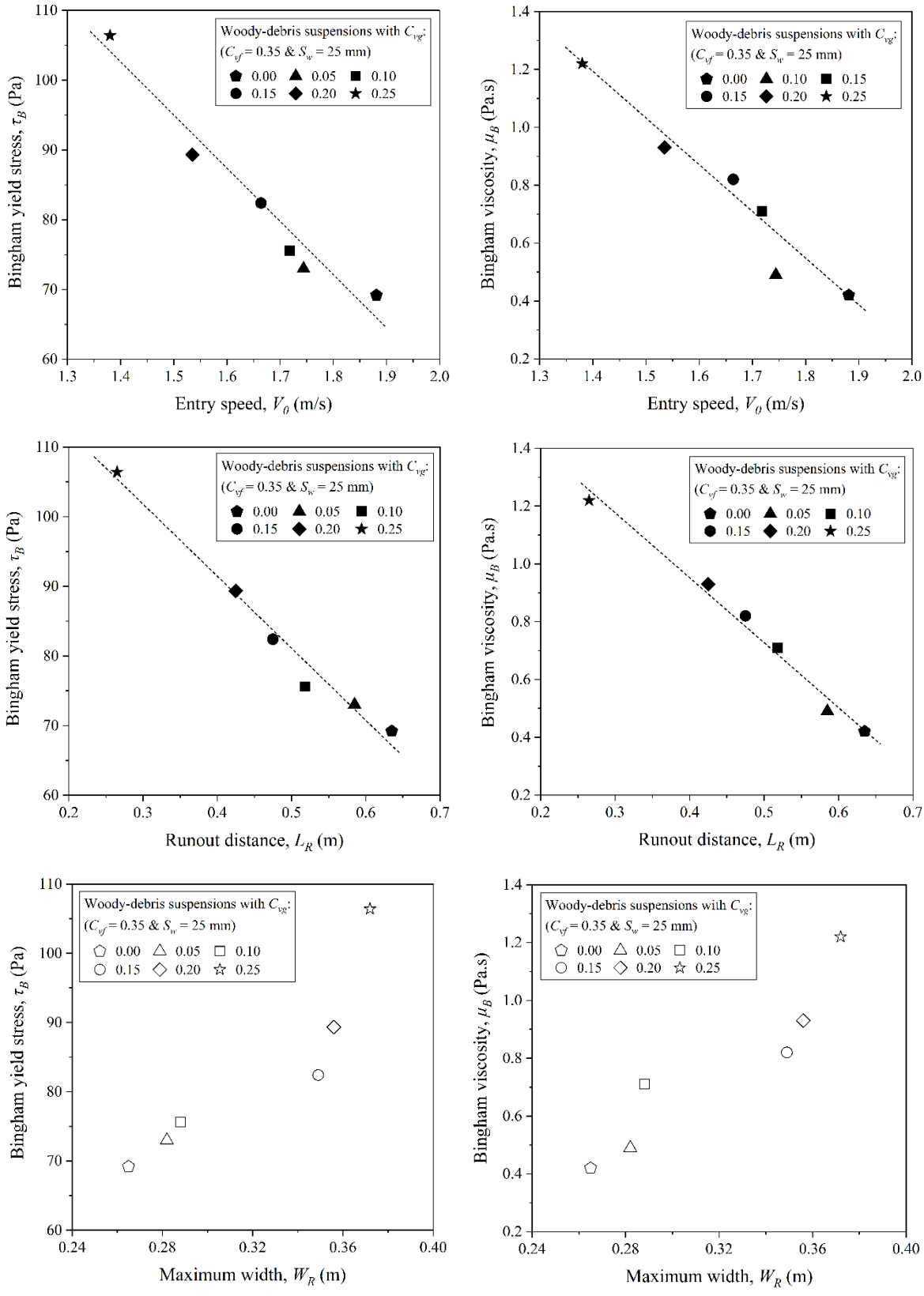

Fig. 14. The relationships between rheological parameters and inclined channel test parameters of woody-debris suspensions with C_{vf} = 0.35 and S_w = 25 mm but different C_{vg}.

Table 4. The correlations between the rheological parameters and inclined channel test parameters of woody-debris suspensions.

Correlation model	Coefficients of model		Coefficient of determination, R^2
	a	b	
$\tau_B = aV_0 + b$	-76.30	208.84	0.96
$\mu_B = aV_0 + b$	-1.64	3.47	0.94
$\tau_B = aL_R + b$	-103.16	132.57	0.98
$\mu_B = aL_R + b$	-2.31	1.87	0.98
$\tau_B = aW_R + b$	271.30	-3.80	0.81
$\mu_B = aW_R + b$	6.04	-1.16	0.87

4.6. Mechanisms governing flow and deposition

The experimental results from both the inclined channel tests and rheological measurements are governed by mechanisms related to the flow and deposition of woody-debris suspensions behaving as yield stress fluids. Their behavior could be interpreted within the 1-D depth-averaged momentum framework widely used for yield-stress geophysical flows [1, 41]:

$$\frac{\partial(hu)}{\partial t} + \frac{\partial}{\partial x}\left(hu^2 + \frac{1}{2}gh^2\cos\theta\right) = gh\sin\theta - \frac{\tau_b}{\rho} \tag{16}$$

where the gravitational driving term ($gh\sin\theta$) is balanced by the basal resistance τ_b/ρ. For a Bingham fluid, τ_b combines a constant yield component τ_B and a viscous component typically expressed using closure relations of the form $\mu_B(u/h)$ in steady or slowly varying conditions [41].

4.6.1. Entry speed (V_0) and flow along the inclined channel

Along the 20° inclined channel, the released 2 liters volume rapidly accelerates and then reaches a quasi-steady regime, nearly uniform flow over most of the 2 m length, as evidenced by the constant entry speed observed in high-speed recordings. In this regime, the momentum balance is dominated by the competition between gravitational driving and basal resistance:

$$gh\sin\theta \approx \frac{\tau_b}{\rho} \tag{17}$$

Classical theory for homogeneous Bingham fluids indicates that the characteristic flow velocity U scales as [41]:

$$U = \frac{\rho g h^2 \sin\theta}{\mu_B} \times f(\xi), \qquad \xi = \frac{\tau_B}{\rho g h \cos\theta} \tag{18}$$

where $f(\xi)$ is a monotonically decreasing function ($f(0) = 1/3, f \to 0$ as $\xi \to 1$). Although finite volume and particle segregation prevent fully uniform flow, the measured entry speed V_0 (front velocity at channel exit) follows the same qualitative trends. Higher C_{vf} and C_{vg} increase both τ_B and μ_B, thereby reducing V_0 (Figs. 5 & 6). Conversely, longer woody debris (larger S_w) slightly increase V_0 because the elongated particles rapidly align parallel to the flow direction (high-speed imaging), reducing transverse interlocking and effective basal friction, an anisotropic effect that lowers the effective τ_b below the bulk rheological prediction but remains compatible with the underlying momentum balance.

4.6.2. Runout distance (L_R), deposit width (W_R), and deposit thickness (H_R)

Runout and deposit morphology are governed by dissipation of the momentum exported from the channel, set primarily by V_0. Once the flow enters the horizontal tank and the driving term ($gh \sin\theta$) vanishes, the residual motion is arrested by yield-stress resistance. The depth-averaged momentum equation then describes decelerating flow with weak lateral spreading driven by the hydrostatic pressure gradient. For a homogeneous yield-stress fluid of fixed released volume (V) on a horizontal tank, self-similar gravity-current theory predicts the following scaling laws [42]:

$$L_R \propto V^{3/5} \tau_B^{-1/5} \tag{19}$$

$$H_R \propto V^{2/15} \tau_B^{3/5} \tag{20}$$

since $V = 2$ liters is constant, higher bulk yield stress favours shorter runout and thicker deposits, trends clearly observed when C_{vf} or C_{vg} is increased. In the present suspensions, however, strong particle migration produces a woody-debris-rich frontal carpet that dramatically increases local τ_b far beyond bulk values, causing premature arrest. Lateral spreading is strongly inhibited (narrower W_R), and longer woody debris favor downstream alignment, yielding longer but thinner and narrower deposits.

4.6.3. Particle-scale interactions and effective basal resistance

The rheological tests were conducted at a $C_{vf} = 0.35$ and $C_{vg} = 0.0$ - 0.25, corresponding to $C_{vt} = 0.35$ - 0.51 (Table 1). This range places the suspensions in a high-concentration regime dominated by inter-particle contacts [38, 39]. In this regime, the woody debris, characterised by an elongated shape, representative size $S_w = 25$ mm, and low density ≈ 0.28 g/cm^3, act as coarse, non-colloidal inclusions that intensify frictional interactions and jamming with the fine-sediment matrix. The rheological trends are fully consistent with homogenization theories for non-colloidal inclusions in yield-stress fluids, which predict that the relative yield stress diverges as the inclusion volume fraction approaches the maximum packing fraction [38, 39]:

$$\frac{\tau_B}{\tau_{B0}} \approx \left(1 - \frac{C_{vg}}{C_{vg\text{-}max}}\right)^{-\alpha}, \qquad (\alpha \approx 2) \tag{21}$$

The collapse of the present data in Fig. 13a gives $C_{vg\text{-}max} \approx 0.58$. The elongated shape and low density of woody debris significantly reduce $C_{vg\text{-}max}$ relative to spherical particles (typically

$C_{vg\text{-}max} \approx 0.62$ - 0.64 [17, 38, 39]), thereby amplifying both τ_B and μ_B, leading to an exceptionally steep increase compared with the behavior of spherical beads at the same volume fraction. This friction-dominated rheology increases the effective τ_b/ρ and explains the pronounced reductions in V_0 and L_R as C_{vg} increases (Figs. 5 & 10).

5. CONCLUSIONS

This study presents an indirect approach for estimating the rheological characteristics of woody-debris suspensions using an inclined channel test. By using woody-debris suspensions with varying fine-sediment fraction (C_{vf}), woody debris proportion (C_{vg}), and woody debris size (S_w), comprehensive analyses were conducted through both inclined channel tests and rheometer measurements. These analyses aimed to investigate the flow behavior (e.g., entry speed) deposit characteristics (e.g., runout distance, deposit width, deposit thickness, and final profile) and rheological properties (e.g., yield stress and viscosity). Experiments were conducted across a range of material compositions and particle sizes ($0.25 \le C_{vf} \le 0.35$, $0 \le C_{vg} \le 0.25$, $10 \le S_w \le 55$ mm). The key findings and conclusions of this study are summarized as follows:

1. The entry speed systematically increases as the fine-sediment fraction (C_{vf}) and woody debris proportion (C_{vg}) decrease, and as the woody debris size (S_w) increases. This results in a greater runout distance and deposit thickness, while the deposit width decreases. Among these deposit parameters, the runout distance exhibits higher sensitivity to variations in deposit width and thickness.
2. The rheological parameters, including Bingham yield stress and viscosity, are significantly influenced by the proportion of woody debris in the sediment suspensions. Higher proportions of woody debris result in increasing values for these parameters.
3. The rheological parameters exhibit a strong correlation with inclined channel test parameters, highlighting the potential of using inclined channel tests as an indirect method for estimating the rheological properties of concentrated debris flows containing the larger woody debris.
4. To gain a more comprehensive understanding of woody-debris suspension rheology and its relationship with inclined channel test parameters, further research should consider expanding the experimental range of fine-sediment fractions (C_{vf}) and woody debris sizes (S_w) in rheometer measurements.

Author Contributions: Conceptualization, Chyan-Deng Jan, Le-Trang Nguyen; Format analysis, Chyan-Deng Jan, Le-Trang Nguyen; Investigation, Le-Trang Nguyen; Supervision, Chyan-Deng Jan; Writing-original draft, Le-Trang Nguyen; Writing-review & editing, Chyan-Deng Jan, Le-Trang Nguyen.

Data Availability Statement: The raw data of this article will be made available by the authors on request.

Acknowledgement: The authors gratefully acknowledge the financial support provided by the National Science and Technology Council, Taiwan (Project No.: NSTC 114-2625-M-006-006).

Conflict of interest: The authors have no relevant financial or non-financial interests to disclose.

REFERENCES

[1] Iverson, R. M. (1997). The physics of debris flows. *Reviews of Geophysics*, 35(3), 245-296. https://doi.org/10.1029/97RG00426

[2] Takahashi, T., & Das, D. K. (2014). *Debris flow: Mechanics, prediction and countermeasures* (2nd ed.). CRC Press. https://doi.org/10.1201/b16647

[3] Benda, L., & Dunne, T. (2003). Stochastic forcing of sediment supply to channel networks from landsliding and debris flow. *Water Resources Research*, 39(11), 1311. https://doi.org/10.1029/97WR02388

[4] Iverson, R. M., Logan, M., LaHusen, R. G., & Berti, M. (2010). The perfect debris flow? Aggregated results from 28 large-scale experiments. *Journal of Geophysical Research: Earth Surface*, 115(F3). https://doi.org/10.1029/2009JF001514

[5] Major, J. J., & Iverson, R. M. (1999). Debris-flow deposition: Effects of pore-fluid pressure and friction concentrated at flow margins. *Geological Society of America Bulletin*, 111(10), 1424-1434. https://doi.org/10.1130/0016-7606(1999)111<1424:DFDEOP>2.3.CO;2

[6] Chateau, X., Ovarlez, G., & Trung, K. L. (2008). Homogenization approach to the behavior of suspensions of noncolloidal particles in yield stress fluids. *Journal of Rheology*, 52(2), 489-506. https://doi.org/10.1122/1.2838254

[7] Ducloué, L., Pitois, O., Goyon, J., Chateau, X., Ovarlez, G. (2015). Rheological behaviour of suspensions of bubbles in yield stress fluids. *Journal of Non-Newtonian Fluid Mechanics*, 215, 31-39. https://doi.org/10.1016/j.jnnfm.2014.10.003

[8] Stickel, J. J., & Powell, R. L. (2005). Fluid mechanics and rheology of dense suspensions. *Annual Review of Fluid Mechanics*, 37, 129-149. https://doi.org/10.1146/annurev.fluid.36.050802.122132

[9] Barnes, H. A., & Nguyen, Q. D. (2001). Rotating vane rheometry - A review. *Journal of Non-Newtonian Fluid Mechanics, 98*(1), 1-14. https://doi.org/10.1016/S0377-0257(01)00095-7

[10] Kaitna, R., Palucis, M. C., Yohannes, B., Hill, K. M., & Dietrich, W. E. (2016). Effects of coarse grain size distribution and fine particle content on the rheology of debris-flow material. *Journal of Geophysical Research: Earth Surface, 121*(3), 544-563. https://doi.org/10.1002/2015JF003725

[11] Major, J. J., & Pierson, T. C. (1992). Debris flow rheology: Experimental analysis of fine-grained slurries. *Water Resources Research*, 28(3), 841-857. https://doi.org/10.1029/91WR02834

[12] Coussot, P., Proust, S., & Ancey, C. (1996). Rheological interpretation of deposits of yield stress fluids. *Journal of Non-Newtonian Fluid Mechanics*, 66(1-2), 55-70. https://doi.org/10.1016/0377-0257(96)01474-7

[13] Lancaster, S. T., Hayes, S. K., & Grant, G. E. (2003). Effects of wood on debris flow runout in small mountain watersheds. *Water Resources Research*, 39(6), 1168. https://doi.org/10.1016/0377-0257(96)01474-7

[14] Coussot, P., & Meunier, M. (1996). Recognition, classification, and mechanical description of debris flows. *Earth-Science Reviews*, 40(3-4), 209-227. https://doi.org/10.1016/0012-8252(95)00065-8

[15] Jan, A., & Dey, S. (2022). Slump test for estimating debris flow rheology: A review. *Natural Hazards*, 114(1), 45-68. https://doi.org/10.1016/j.euromechflu.2024.04.005

[16] Ancey, C., & Jorrot, H. (2001). Yield stress for particle suspensions within a clay dispersion. *Journal of Rheology*, 45(2), 297-319. https://doi.org/10.1122/1.1343879

[17] Dey, L., Jan, C. D., & Wang, J. S. (2021). Effects of particle fractions on the Bingham yield stress and viscosity of fine-coarse particle suspensions. *Journal of Mountain Science*, 18(11), 1960-1970. https://doi.org/10.1007/s11629-021-6881-5

[18] Kaitna, R., Palzer, M., & Hutter, K. (2007). Rheological properties of granular and slurry-type dense snow avalanches. *Cold Regions Science and Technology*, 49(2), 104–114. https://doi.org/10.1016/j.coldregions.2007.01.003

[19] Banfill, P. F. G. (2006). Rheology of fresh cement and concrete. *In Rheology Reviews 2006. British Society of Rheology*. 61-130. http://www.bsr.org.uk/rheology-reviews/RheologyReviews/fresh-cement-concrete-Banfill.pdf

[20] Jiao, D., Shi, C., Yuan, Q., An, X., Liu, Y., & Li, H. (2017). Effect of constituents on rheological properties of fresh concrete - A review. *Cement and Concrete Composites*, 83, 146-159. https://doi.org/10.1016/j.cemconcomp.2017.07.016

[21] Leighton, D., & Acrivos, A. (1987). The shear-induced migration of particles in concentrated suspensions. *Journal of Fluid Mechanics*, 181, 415-439. https://doi.org/10.1017/S0022112087002155

[22] Phillips, R. J., Armstrong, R. C., Brown, R. A., Graham, A. L., & Abbott, J. R. (1992). A constitutive equation for concentrated suspensions that accounts for shear-induced particle migration. *Physics of Fluids A: Fluid Dynamics*, 4(1), 30-40. https://doi.org/10.1063/1.858498

[23] Nguyen, Q.D., & Boger, D.V. (1983). Yield stress measurement for concentrated suspensions. *Journal of Rheology*, 27 (4), 321-349. https://doi.org/10.1122/1.549709

[24] Fisher, D.T., Clayton, S.A., Boger, D.V., & Scales, P.J. (2007). The bucket rheometer for concentrated suspensions. *In: Proceedings of the 16th International Congress on Rheology*, 271-273.

[25] Koehler, E. P., & Fowler, D. W. (2004). Development of a Portable Rheometer for Fresh Portland Cement Concrete (M.S. thesis). Aggregates Foundation for Technology, Research and Education (AFTRE), The University of Texas at Austin, 1-138. http://hdl.handle.net/2152/35338

[26] Güneyisi, E., Gesoglu, M., Naji, N., & İpek, S. (2016). Evaluation of the rheological behavior of fresh self-compacting rubberized concrete by using the Herschel–Bulkley and modified Bingham models. *Archives of Civil and Mechanical Engineering*, 16(1), 9-19. https://doi.org/10.1016/j.acme.2015.09.003

[27] Scotto di Santolo, A., Pellegrino, A.M., Evangelista, A., & Coussot, P. (2012). Rheological behaviour of reconstituted debris-flow material. *Geotechnique*, 62 (1), 19-27. https://doi.org/10.1680/geot.10.P.005

[28] Jan, C. D., Nguyen, L. T., & Dey, L. (2025). Effects of grain size distribution on the movement and deposition of granular materials flowing down an inclined channel. *Journal of Mechanics, 41*, 157-172. https://doi.org/10.1093/jom/ufaf012

[29] de Haas, T., Braathen, A., & Blikra, L. H. (2015). Effects of debris flow composition on runout, depositional mechanisms, and deposit morphology in laboratory experiments. *Journal of Geophysical Research: Earth Surface*, 120(12), 2631-2648. https://doi.org/10.1002/2015JF003525

[30] Pellegrino, A. M., Scotto di Santolo, A., & Schippa, L. (2015). An integrated procedure to evaluate rheological parameters to model debris flows. *Engineering Geology*, 196, 88-98. https://doi.org/10.1016/j.enggeo.2015.07.002

[31] Chang, H., Ryou, K., & Lee, H. (2021). Debris Flow Characteristics in Flume Experiments Considering Berm Installation. *Applied Sciences*, 11(5), 2336. https://doi.org/10.3390/app11052336

[32] Wang, D., Wang, X., Chen, X., Lian, B., & Wang, J. (2022). Analysis of factors influencing the large wood transport and block-outburst in debris flow based on physical model experiment. *Geomorphology*, 398, 108054. https://doi.org/10.1016/j.geomorph.2021.108054

[33] Rengers, F. K., McGuire, L. A., Barnhart, K. R., Youberg, A. M., Cadol, D., Gorr, A. N., Hoch, O., Beers, R., & Kean, J. W. (2023). Influence of large woody debris on Post-Wildfire Debris Flow Sediment Storage. *Natural Hazards and Earth System Sciences*, 23, 2075-2088. https://doi.org/10.5194/egusphere-2022-1398

[34] Matioli, A. S., Bezerra, F. H., & Costa, C. L. (2013). Influence of woody debris on debris flow viscosity and flow dynamics. *Geophysical Research Letters*, 40(24), 6196-6201. https://doi.org/10.1002/2013GL058263

[35] Braudrick, C. A., & Grant, G. E. (2001). Transport and deposition of large woody debris in streams: A flume experiment. *Geomorphology*, 41(4), 263-283. https://doi.org/10.1016/S0169-555X(01)00058-7

[36] Nakamura, F., Seo, J. I., Akasaka, T., & Swanson, F. J. (2017). Large wood, sediment, and flow regimes: Their interactions and temporal changes caused by human impacts in Japan. *Geomorphology*, 279, 176-187. https://doi.org/10.1016/j.geomorph.2016.11.001

[37] Phillips, C., & Davies, T. H. (1991). Determining rheological parameters of debris-flow material. *Geomorphology*, 4(2), 101-110. https://doi.org/10.1016/0169-555X(91)90022-3

[38] Mahaut, F., Chateau, X., Coussot, P., & Ovarlez, G. (2008). Yield stress and elastic modulus of suspensions of noncolloidal particles in yield stress fluids. *Journal of Rheology*, 52(1), 287-313. https://doi.org/10.1122/1.2798234

[39] Ovarlez, G., Mahaut, F., Deboeuf, S., Lenoir, N., Hormozi, S., & Chateau, X. (2015). Flows of suspensions of particles in yield stress fluids. *Journal of Rheology*, 59, 1449-1486. https://doi.org/10.1122/1.4934363

[40] Cohen, J., Cohen, P., West, S.G., & Aiken, L.S. (2003). Applied Multiple Regression/Correlation Analysis for the Behavioral Sciences (3rd ed.). *Routledge*. https://doi.org/10.4324/9780203774441

691 [41] Ancey, C. (2007). Plasticity and geophysical flows: A review. *Journal of Non-Newtonian*
692 *Fluid Mechanics*, 142(1-3), 4-35. https://doi.org/10.1016/j.jnnfm.2006.05.005

693 [42] Coussot, P., & Proust, S. (1996). Slow, unconfined spreading of a mudflow. *Journal of*
694 *Geophysical Research: Solid Earth*, 101(B11), 25251-25266. https://doi.org/10.1029/96JB02486